RSC Advances

PAPER

View Article Online
View Journal | View Issue

Cite this: *RSC Adv.*, 2025, **15**, 11098

Advanced synthesis and multifaceted characterization of a 4,4-diaminodiphenylmethane-melamine-formaldehyde terpolymer: anti-corrosion performance and antimicrobial potential in 1 M hydrochloric acid

Rashmi Sehrawat,[a] Priya Vashishth,[a] Neera Raghav,[b] Anjaneyulu Bendi,[c] A. Jafar Ahamed,[d] N. Mujafarkani*[d] and Bindu Mangla*[a]

Received 14th February 2025
Accepted 17th March 2025

DOI: 10.1039/d5ra01095k

rsc.li/rsc-advances

Herein, a 4,4-diaminodiphenylmethane-melamine-formaldehyde (DMF) terpolymer was synthesized and characterized to investigate its anti-corrosion properties for mild steel in a 1 M hydrochloric acid electrolyte. The DMF terpolymer produced through condensation polymerization was characterized using FTIR, ^{1}H NMR, ^{13}C NMR, and gel permeation chromatography. Electrochemical tests showed that it achieved 94% inhibition efficiency at 100 ppm, functioning as a mixed-kind inhibitory agent. The adsorption phenomenon conformed to the paradigms delineated by the Langmuir adsorption isotherm, indicating strong binding through physical and chemical interactions. AFM confirmed the creation of a protective barrier on the steel substrate, while DFT studies supported its molecular adhesion. Additionally, the terpolymer exhibited antimicrobial activity against *Staphylococcus aureus*, *Pseudomonas aeruginosa*, and *Bacillus subtilis*.

1. Introduction

Mild steel is a prevalent ferrous alloy used in fabrication processes owing to its impressive mechanical strength and low economical cost. However, its susceptibility to deterioration causes serious issues for practical applications.[1,2] The surface of the metal corrodes quickly in acidic situations. The pickling method, which uses hydrochloric acid, is commonly used to minimize this problem. HCl is preferred over alternative acids because it is effective in surface smoothing of mild steel and oxide layer elimination while following recognized commercial protocols. However, mild steel inevitably corrodes owing to the harshness of the acid causing stress to the mild steel.[3,4] Air, moisture, and other chemical exposures may also lead to corrosion. As a consequence, mild steel corrosion may culminate in significant mortality and substantial monetary damage.[5] Hence, it is critical to create effective solutions that stop or slow down carbon steel corrosion. Owing to their requirement of low dose and increased effectiveness, corrosion inhibitors are utilized extensively to slow down the pace of corrosion in mild steel.[6,7]

The implementation of corrosion inhibiting substances is a very successful tactic in addressing the formerly described corrosion problem. The majority of these inhibitory agents are organic substances with heteroatoms made up of components including nitrogen, oxygen, and sulphur.[8,9] Furthermore, efficient binding over the steel surface is enabled because of the inclusion of aromatic rings and multiple bonds.[10,11] After being adsorbed, such inhibitors provide a strong shield that defends the surroundings from corrosive substances. In numerous industrial settings, efficient anti-corrosion agents increase the longevity of mild steel structures and improve their operating reliability and cost-effectiveness.[12,13]

Polymers are regarded as promising anti-corrosion agents owing to their favorable environmental and economic benefits, coupled with superior corrosion inhibition properties compared with basic organic substances.[14,15] Polymers offer an extensive surface area coverage on metallic substances, developing a protective layer at the interface that shields the surface from corrosion. Recent studies have investigated the corrosion inhibition effects of various natural and synthetic polymers in different environments.[16,17] The study demonstrates that the distinct molecular and electrical structures, chemical makeup,

[a]*Corrosion Testing Research Lab, Department of Chemistry, J.C. Bose University of Science and Technology, YMCA Faridabad 121006, Haryana, India. E-mail: bindumangla@gmail.com*

[b]*Department of Chemistry, Kurukshetra University, Kurukshetra, 136118 Haryana, India*

[c]*Innovation and Translational Research Hub (iTRH) & Department of Chemistry, Presidency University, Rajanukunte, Itgalpura, Bangalore, 560064, Karnataka, India*

[d]*PG and Research Department of Chemistry, Jamal Mohamed College (Autonomous), (Affiliated to Bharathidasan University), Tiruchirappalli, 620020, Tamilnadu, India. E-mail: nm@jmc.edu*

and macromolecular mass of polymers all affect their efficiency.[18]

B. A. Farzana *et al.* studied the anti-corrosive action of *p*-semidine-guanidine-formaldehyde terpolymer for mild steel using electrochemical and gravimetry techniques.[19] It was found to exhibit 93.7% efficacy at 10^{-3} M in sulphuric acid medium. The adsorption behaviour was elucidated and found to follow the Langmuir isotherm. Additionally, density functional theory (DFT) analysis was conducted to further support and complement the experimental results. In another study, two polymers were used as anti-corrosive agents for mild steel using electrochemical measurements in 1 M HCl: poly(-acrylonitrile) sodium salt (PANa) and poly(acrylic acid) (PAA).[20] They were found to show 91.5% and 95.5% efficacy for PANa and PAA, respectively. Both polymers showed a mixed-kind of inhibition, and the Langmuir isotherm was followed in the adsorption process. The corrosion inhibition processes were elucidated using SEM and EDAX investigations, and the most reactive locations over the polymers were found through theoretical calculations, which further enhanced the comprehension of the polymer's efficacy as corrosion inhibitors. M. Abdallah *et al.* investigated the inhibiting potential of polymer compounds, poloxamer (PLX) and pectin (PEC), against the degradation of carbon steel in harsh environments using weight loss and electrochemical methods.[21] Lower temperature (298 K) and greater polymer concentration (500 ppm) led to a spike in the inhibitory effectiveness, *i.e.*, 84% and 91% for PLX and PEC, respectively. Both polymers created an adsorptive protective layer to keep the corrosive medium from interacting with the steel surface. Chemical and physical adsorption proceeded in accordance with the Freundlich isotherm. PEC demonstrated more inhibition than PLX, which can be explained by its better surface coverage owing to its larger molar mass. All techniques produced findings with consistent inhibition.

Earlier research shows that polymers exhibit excellent adsorption properties and strong interactions with metal surfaces. However, limited studies have focused on terpolymer resins, particularly in hydrochloric acid media. This study addresses this gap by exploring the anti-corrosive properties of 4,4-diaminodiphenylmethane-melamine-formaldehyde terpolymer (DMF), employing both experimental and computational approaches to provide a comprehensive understanding of its corrosion inhibition mechanism.

The novelty of this terpolymer lies in its cost-effectiveness, multifunctional properties, and ease of synthesis. It is derived from readily available and low-cost raw materials, making it a viable option for large-scale applications in biological evaluation, thermal degradation, ion-exchange, and anti-corrosive studies. Additionally, the condensation polymerization process only requires simple reaction conditions, eliminating the need for complex synthesis procedures. This not only enhances its practicality and scalability but also makes it an environmentally and economically favorable candidate for industrial applications.

In this study, a terpolymer (DMF) was synthesized through condensation polymerization of 4,4-diaminodiphenylmethane and melamine with formaldehyde. The synthesized DMF terpolymer was characterized using FTIR, ^{1}H and ^{13}C NMR techniques. The average molecular weight of the DMF polymer was ascertained through gel permeation chromatography. The polymer was then tested for anti-corrosion characteristics for mild steel in a 1 M HCl solution utilizing potentiodynamic polarization, linear polarization resistance, and electrochemical impedance spectroscopy. The adsorption capacity of the DMF terpolymer was further analysed through AFM surface studies. Additionally, DFT calculations were employed to explore the relationship between the DMF terpolymer's structure and its experimental effectiveness. Furthermore, the antimicrobial activity of the terpolymeric ligand was assessed through the disc diffusion method against *Staphylococcus aureus*, *Pseudomonas aeruginosa*, and *B. subtilis*.

2. Experimental

2.1. Material and methods

All of the chemicals utilized in this study were obtained from Sigma-Aldrich and were of analytical reagent (AR) grade due to their highest quality. Using KBr pellets and an ABB MB3000 instrument, IR spectra were acquired encompassing a range of 400 to 4000 cm^{-1}. A Bruker apparatus running at 400 MHz was used for NMR studies with $CDCl_3$ as the solvent. The corrosion investigation employed a mild steel working electrode constructed with an estimated area of 10 cm^2, measuring 5 cm by 2 cm. The samples were sourced from a nearby marketplace and their elemental makeup by weight was as follows: 0.14% carbon, 0.20% nickel, 0.10% silicon, 0.14% copper, 0.15% manganese, and the balance content was iron (Fe). Emery sheets varying in grit counts were used to smooth and clean the specimen's surface to guarantee a consistent surface for corrosion assessment. After that, the samples were meticulously cleaned employing doubly distilled water, then acetone washing and thorough drying according to ASTM protocols. The 1 M HCl solution, which was constantly employed across the investigation, was created by mixing the strong acid with double-distilled water. Furthermore, various amounts of the inhibitory agent DMF terpolymer (20–120 ppm) were dissolved in this solution of acid. The homogeneous solutions were adequately stirred to ensure complete dissolution and uniform dispersion before conducting the experiments.

2.2. Synthesis of 4,4-diaminodiphenylmethane-melamine-formaldehyde terpolymer (DMF)

A mixture of 4,4-diaminodiphenylmethane (0.025 mole) and melamine (0.025 mole) with formaldehyde (0.075 mole) was added to a round bottom flask and refluxed in an oil bath at 130 °C for 6 h in presence of dimethylformamide (Scheme 1).[22] The content of the flask was periodically shaken well to ensure homogeneous mixing. After the stipulated reaction time, the content of the flask was poured into a beaker containing ice crystals with vigorous shaking and kept overnight. The separated resin was washed with warm water. The resin was air dried and extracted with ether to remove unreacted monomers. The resin was purified twice by dissolving in 1 : 1 (HCl/water) and regenerated by the addition of

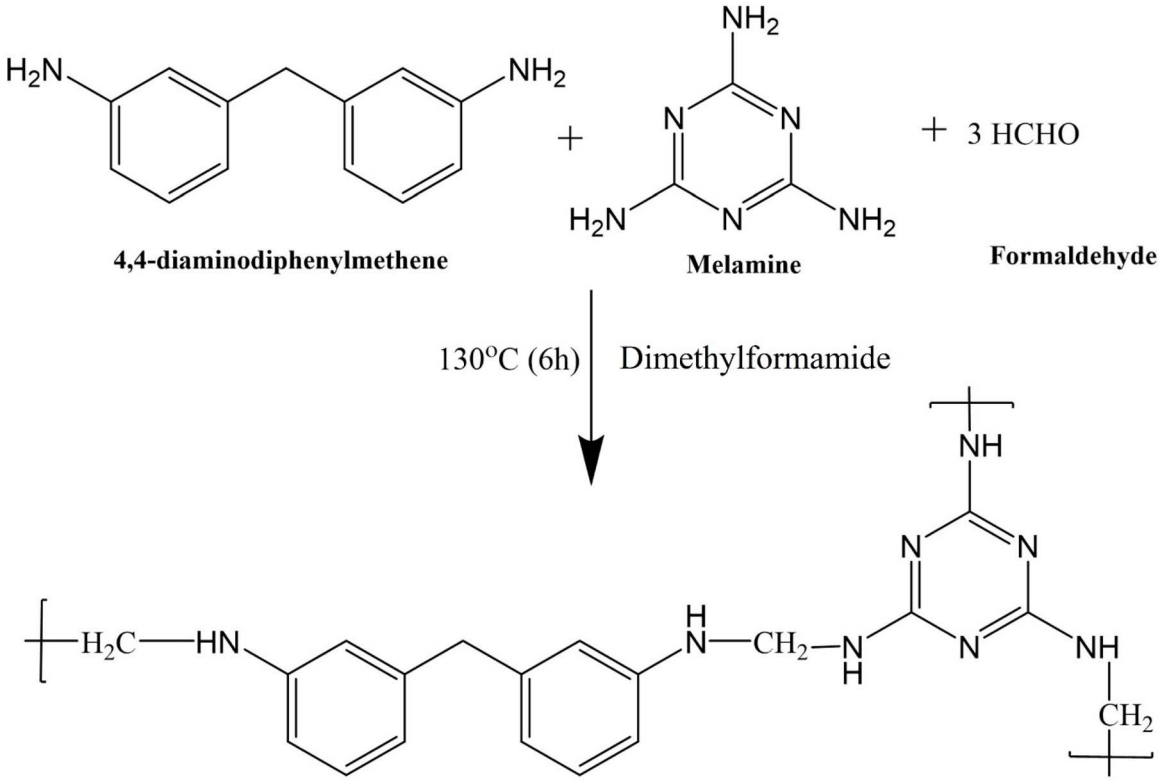

Scheme 1 Synthesis of 4,4-diaminodiphenylmethane-melamine-formaldehyde terpolymer (DMF).

15% NaOH with constant stirring. The resin was filtered off, washed with hot water, methanol, and acetone and air dried at 60 °C for 6 hours in a hot air oven. The synthesised resin was then characterised using FTIR, ^{1}H NMR and ^{13}C NMR.[23,24] The average molecular weight of the DMF terpolymer was determined using gel permeation chromatography.

2.3. Corrosion study

2.3.1. Electrochemical study. The electrochemical measurements were carried out at ambient temperature on a mild steel substrate (working electrode) in a three-electrode configuration (working, reference, and counter electrodes) by employing a GAMRY potentiostat workstation (IFC-1010-28152). The reference electrode was a platinum wire and the counter electrode was an Ag/AgCl electrode. In the cell assembly, the mild steel surface, which has an apparent area of 1 cm^2, served as a working electrode. The mild steel was allowed to spontaneously degrade in the hostile acidic settings for 1 h, refrained from the introduction of an exterior voltage with the objective to produce a steady open circuit potential (OCP). The voltage band which was implemented to correctly interpret the linear polarization graphs was −0.02 V to +0.02 V.[25] The linear polarization resistance and the computation of the mitigation consequences of DMF inhibitor in such experiments were determined using the equation below at a scan velocity of 1 mV s^{-1}:

$$\mathrm{IE\%} = \frac{R_p' - R_p^\circ}{R_p^\circ} \times 100$$

where IE% is the inhibition efficiency and R_p' and $R_p^\circ R_p^\circ$ are the polarization resistances in inhibited and inhibitor-free settings, respectively.

The excitation signal's amplitude factor has been configured to 10 mV throughout the electrochemical impedance spectroscopy (EIS) examination, and the EIS's sweeping frequency band has been adjusted to 10^{-2}–10^{5} Hz. Using electrochemical variables (R_{ct}), the inhibitory efficacy may be computed as follows:

$$\mathrm{IE\%} = \frac{\left(R_{ct}' - R_{ct}^\circ\right)}{R_{ct}'} \times 100$$

where R_{ct}' and R_{ct}° are inhibited and inhibitor-free resistance to charge transfer settings, respectively.

Using polarization tests, the consequences of inhibition on mild steel dissolution were researched at 1 mV s^{-1} sweeping among a cathodic potential of −0.25 V and anodic potential of +0.25 V. The effectiveness of compound prevention was determined using the formula below:

$$\mathrm{IE\%} = \frac{I_{corr}^\circ - I_{corr}'}{I_{corr}^\circ} \times 100$$

where I_{corr}' and I_{corr}° are inhibited and inhibitor-free corrosion current densities, respectively.

The concentration range of DMF polymer was selected between 20–100 ppm, as there was no significant improvement in the inhibition efficiency beyond 100 ppm. This indicates that the polymer had reached its maximum inhibitory effect at 100 ppm, making further increases in concentration unnecessary.

2.3.2. Surface study: AFM. By characterizing the surface of steel samples (10 × 10 cm) prior to and subsequent to corrosion inhibition using atomic force microscopy (AFM), the adsorption of inhibitors was confirmed. The specimens were submerged in 1.0 M HCl for 3 h at 308 K with and without the optimum concentration (100 ppm) of the DMF terpolymer inhibitor. A Bruker atomic force microscope was used for the detection of surface roughness before and after inhibition.

2.3.3. Theoretical study: DFT. One plausible and useful approach for estimating the performance of corrosion inhibitor molecules is to use theoretical techniques such as density functional theory (DFT). The density functional theory (DFT) employing the B3LYP functional and the 6-311++G(d, p) basis set was applied in this study's computations, which was executed utilizing the Gaussian 16 software package. In this investigation, the energies of HOMO, LUMO, energy gap (ΔE), and quantum descriptors that include ionization potential (IE), electron affinity (EA), chemical softness (σ), hardness (η), electrophilicity (ω), fraction of electron density transferred (ΔN), and electronegativity (χ) were evaluated for the DMF polymer in both protonated and neutral forms in the gaseous state, using the equations provided below:[26]

$$\Delta E = E_{\mathrm{LUMO}} - E_{\mathrm{HOMO}}$$

$$\mathrm{IE} = -E_{\mathrm{HOMO}}$$

$$\mathrm{EA} = E_{\mathrm{LUMO}}$$

$$\mu = \frac{E_{\mathrm{LUMO}} + E_{\mathrm{HOMO}}}{2}$$

$$\chi = \frac{\mathrm{IE} + \mathrm{EA}}{2}$$

$$\eta = \frac{\mathrm{IE} - \mathrm{EA}}{2}$$

$$\omega = \frac{\mu^2}{2\eta}$$

$$\Delta N = \frac{\chi_{\mathrm{Fe}} - \chi_{\mathrm{inh.}}}{2(\eta_{\mathrm{Fe}} - \eta_{\mathrm{inh}})}$$

Fukui functions were implemented to determine the local reactivity of the inhibitory compounds under study. These functions aid in the identification of reactive regions involved in nucleophilic and electrophilic attacks by assessing shifts in the density of electrons.[27] The Fukui indices of the polymers were computed using simple statistical approaches, providing an analytical foundation for identifying the most favourable places for molecular interactions. The Fukui function was computed using Hirshfeld population analysis for nucleophilic attack (f_k^+) and for electrophilic attack (f_k^-):

$$f_k^+ = q_k(n+1) - q_k(n)$$

$$f_k^- = q_k(n) - q_k(n-1)$$

The charges corresponding to the neutral, positive, and negative states are denoted as $q_k(n)$, $q_k(n+1)$, and $q_k(n-1)$, respectively.

2.4. Antimicrobial study

Plant materials were collected from Trichy, Tamil Nadu, and transported to the laboratory. The leaves were shade-dried at room temperature and ground into a fine powder. Ten grams of the powdered material were extracted using 100 mL of distilled water in a Soxhlet apparatus. The extraction was carried out continuously over seven days at room temperature (31 °C) to ensure complete extraction of the plant's bioactive compounds. After extraction, the liquid was filtered through Whatman No.1 filter paper, and the resulting extract was stored in the refrigerator for further antimicrobial studies.

Bacterial strains, including *Staphylococcus aureus*, *Pseudomonas aeruginosa*, and *Bacillus subtilis*, were obtained from Kirnd Institute of Research and Development, Tiruchirappalli. The strains were maintained on nutrient agar slants at 4 °C. For the antimicrobial assay, bacterial cultures were subcultured in nutrient broth at 37 °C for 8 h to achieve an inoculum concentration of 10^5–10^6 CFU mL^{-1}. The nutrient broth was prepared using standard components peptone (5 g), beef extract (3 g), agar (15 g), sodium chloride (5 g), and yeast extract (1.5 g), excluding agar, and sterilized by autoclaving at 121 °C and 15 psi for 15 min.[28]

To assess antimicrobial activity, the Kirby–Bauer agar well diffusion method was employed. The nutrient agar medium was subjected to sterilization, subsequently aliquoted into aseptically prepared Petri dishes, and permitted to undergo solidification under controlled conditions (Fig. 1). Bacterial cultures were meticulously distributed across the agar plate surfaces *via* uniform swabbing employing sterilized cotton applicators. Wells were created in the agar using a sterile well cutter, and the prepared plant extracts were aseptically added to the wells. The plates were incubated at 37 °C for 24 h and the zones of inhibition around each well were assessed to determine the antimicrobial efficacy of the plant extracts against the test bacterial strains.[29]

3. Results and discussion

3.1. Characterisation of polymer (DMF)

3.1.1. Gel permeation chromatography. The average molecular weight of the DMF polymer was ascertained through gel permeation chromatography. The number average molecule weight (M_n) and weight average molecular weight (M_w) were measured to be 1715 and 1785 respectively. The poly dispersity

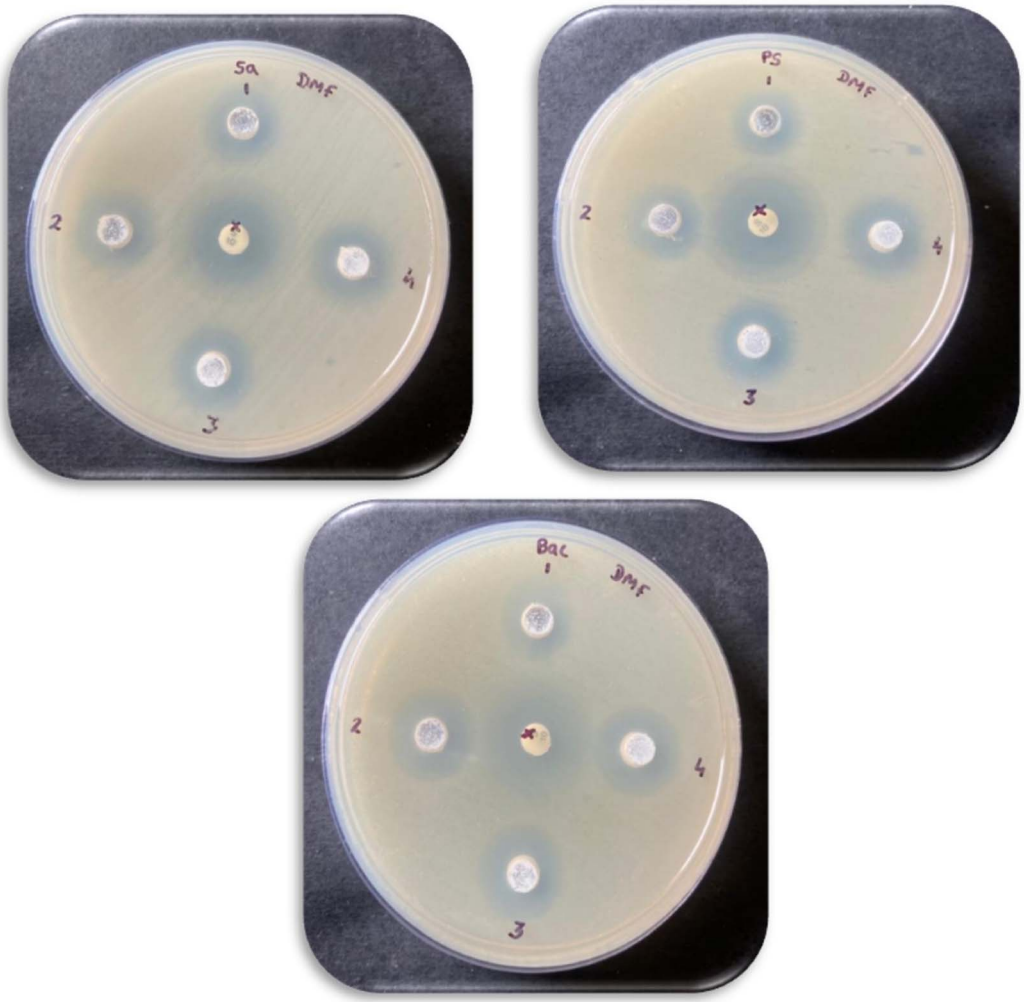

Fig. 1 Antimicrobial screening of DMF terpolymer ligand.

Table 1 Average molecular weight of DMF terpolymer ligand

Compound	M_w	M_n	Polydispersity index M_w/M_n
DMF	1785	1715	1.041

index (M_w/M_n) was calculated to be 1.041. The molecular weight measurement is presented in Table 1.

3.1.2. Infrared spectroscopy. The theoretical infrared (IR) spectral calculations were performed employing the Gaussian 16 software package, utilizing the B3LYP functional in conjunction with the 6-31++G(d, p) basis set within the gas-phase approximation. The experimentally acquired FTIR spectral frequencies were systematically juxtaposed with their theoretically computed counterparts, revealing a strong correlation between the two. The FTIR spectrum of the DMF terpolymer is depicted in Fig. 2 and spectral data are presented in Table 2. The band observed at 3399.11 cm^{-1} can be attributed to the N–H bridge in the terpolymer resin. The band at 3019.41 cm^{-1} is due to the presence of C–H stretching in the aromatic ring. A broad band at 1661.44 cm^{-1} is attributed to the C=C aromatic stretching linkage present in the terpolymer. The band at 1513.49 cm^{-1} is assigned to C=N stretching frequency. The band at 1407.37 cm^{-1} is due to aliphatic C–H stretching. A band at 1243.88 cm^{-1} is assigned to C–N stretching in the terpolymer resin.

3.1.3. NMR spectral studies. The ^{1}H NMR signal at 5.99 (δ) ppm is assigned to the proton of the N–H bridge (Fig. 3). The signal at 6.61–6.95 (δ) ppm is assigned to all the aromatic protons. The signal observed at 2.5 (δ) ppm is assigned to the methylene group.

The ^{13}C NMR spectrum of the DMF terpolymer is depicted in Fig. 3. In the spectrum, the signal at 146.09 (δ) ppm is assigned to the carbon of C=N. The signals at 112.11, 112.92, 113.15, 114.4, 129.37 and 129.64 (δ) ppm were assigned to all the carbons of aromatic rings that are present in diaminodiphenylamine and pyrimidine groups. The signal observed at 59.87 (δ) ppm is assigned to the methylene group present in the terpolymer ligand.

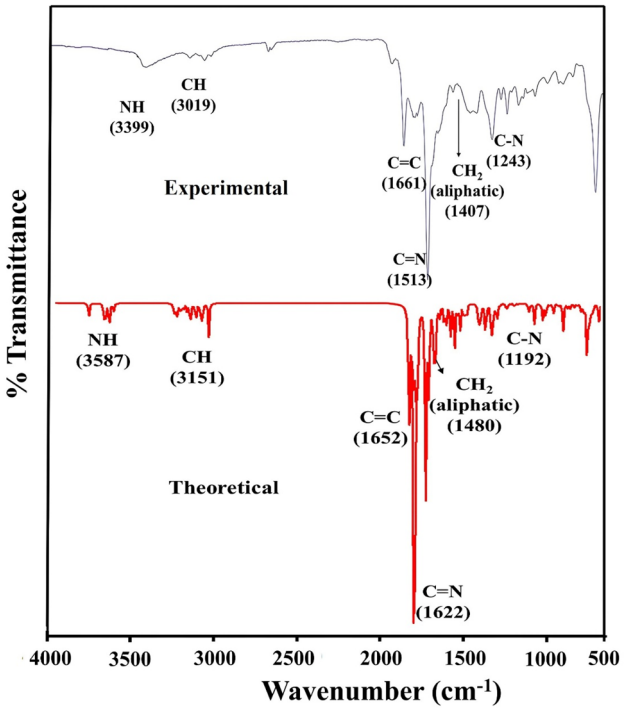

Fig. 2 FTIR spectrum of DMF terpolymer ligand.

Table 2 FTIR spectral data of DMF terpolymer ligand

	Frequency (cm^{-1})	
Vibration mode	Theoretical	Observed
N–H bridge (stretching)	3587	3399.11
Aromatic ring (C–H) stretching	3151	3019.41
Aromatic C=C	1652	1661.44
C=N stretching	1622	1513.49
Aliphatic CH_2 stretching	1480	1407.37
C–N stretching	1192	1243.88

Also, the theoretical ^{1}H and ^{13}C NMR chemical shifts were calculated using the GIAO method with B3LYP/6-31++G(d, p) in the gas phase. The ^{1}H and ^{13}C data for the polymer shown in Table 3 are in good agreement with the experimental values.

3.2. Corrosion study

3.2.1. Electrochemical study

3.2.1.1. OCP. The Open Circuit Potential (OCP) pattern for the steel working electrode submerged in 1.0 M HCl is depicted (Fig. 4), considering the presence and absence of varying DMF inhibitor quantities at 308 K. The OCP of mild steel stabilized after 1 h of immersion within both the blank solution and the solution with the addition of DMF (varying from 20 to 120 ppm). Furthermore, the OCP values with DMF changes to less negative levels relative to the blank 1.0 M HCl solution. The modification is caused by DMF molecules adhering to the steel substrate and preventing steel disintegration. Conversely, the OCP curve moves in a opposite way when DMF is absent, presumably as a result of mild steel dissolving in the anodic phase.

3.2.1.2. Potentiodynamic polarization (PDP) and linear polarization resistance (LPR). By calculating the rate at which mild steel deteriorates, linear polarization resistance (LPR) evaluation aids in the monitoring of corrosion preventive efficacy and permits real-time adjustment of inhibitory agent efficiency. Polarization resistance (R_p) readings for the inhibitor varies from 30.14 Ω cm^2 (for 0 ppm) to 436.2 Ω cm^2 (for 120 ppm). The R_p readings increase as one boosts inhibitor quantity, although I_{corr} (corrosion current density) falls. The inhibition efficacy was 43.56% and 93.09% using 20 ppm and 120 ppm inhibitor, respectively (Table 4). Under acidic settings (1 M HCl), the inhibitors bind onto the metallic surface and create a layer of defence which prevents the interaction of steel and acid. This indicates an obvious link among inhibitor quantity and corrosion management as it leads to greater R_p and diminished I_{corr} readings.

In polarization methods, the cell's current is recorded as the sample potential is modified. In laboratory settings, potentiodynamic polarization (PDP) is widely used because it offers important insights into the processes of corrosion inhibition and the substrate's rate of dissolution in inhibitory situations. To monitor the progression and dynamics of cathode and anode procedures and for evaluating the effect of corrosion inhibiting agent doses upon such reactions, PDP investigations were conducted. The PDP curves of mild steel in 1 M hydrochloric acid, including and excluding distinct inhibitor amounts (20–120 ppm) at 308 K, are displayed in Fig. 5. E_{corr}, I_{corr}, and the Tafel constants (β_a and β_c), which are obtained from the Tafel anodic and cathodic extrapolation area electrochemical elements were computed from the graph. Additionally, Table 5 presents an assessment and summary of the efficiency of the inhibiting agents.

When the inhibitor DMF was incorporated, all of the graphs in Fig. 5 moved in the direction of lesser corrosion current densities (I_{corr}) in contrast to the PDP graph in the uninhibited settings. The comparatively unchanged Tafel slopes imply that the inhibitor influences the pace of corrosion instead of changing the basic electrochemical processes of deterioration, mainly by lowering the I_{corr}. The adhesion of inhibitory molecules over the metallic substrate and the emergence of an inhibitory barrier are responsible for these variations in the I_{corr}. Table 5 analysis shows that increasing inhibitor quantities slows down steel dissolution as the I_{corr} drops significantly as one boosts inhibitor dosage. This suggests that the inhibitor slowed down the speed of deterioration.

Earlier studies characterized inhibitory agents as cathodic or anodic based on a modification in corrosion potential (E_{corr}) exceeding ± 85 mV and a mixed type when this modification is beneath ± 85 mV relative to the inhibitor-free settings.[30] For the present investigation, the highest variation for inhibitor was below ± 85 mV. The data indicates that the action of the inhibitor while binding to metallic substrate is a mixed type, based on their constrained modifications over oxidative and reductive processes while maintaining an E_{corr} value close to the inhibitor-free solutions.

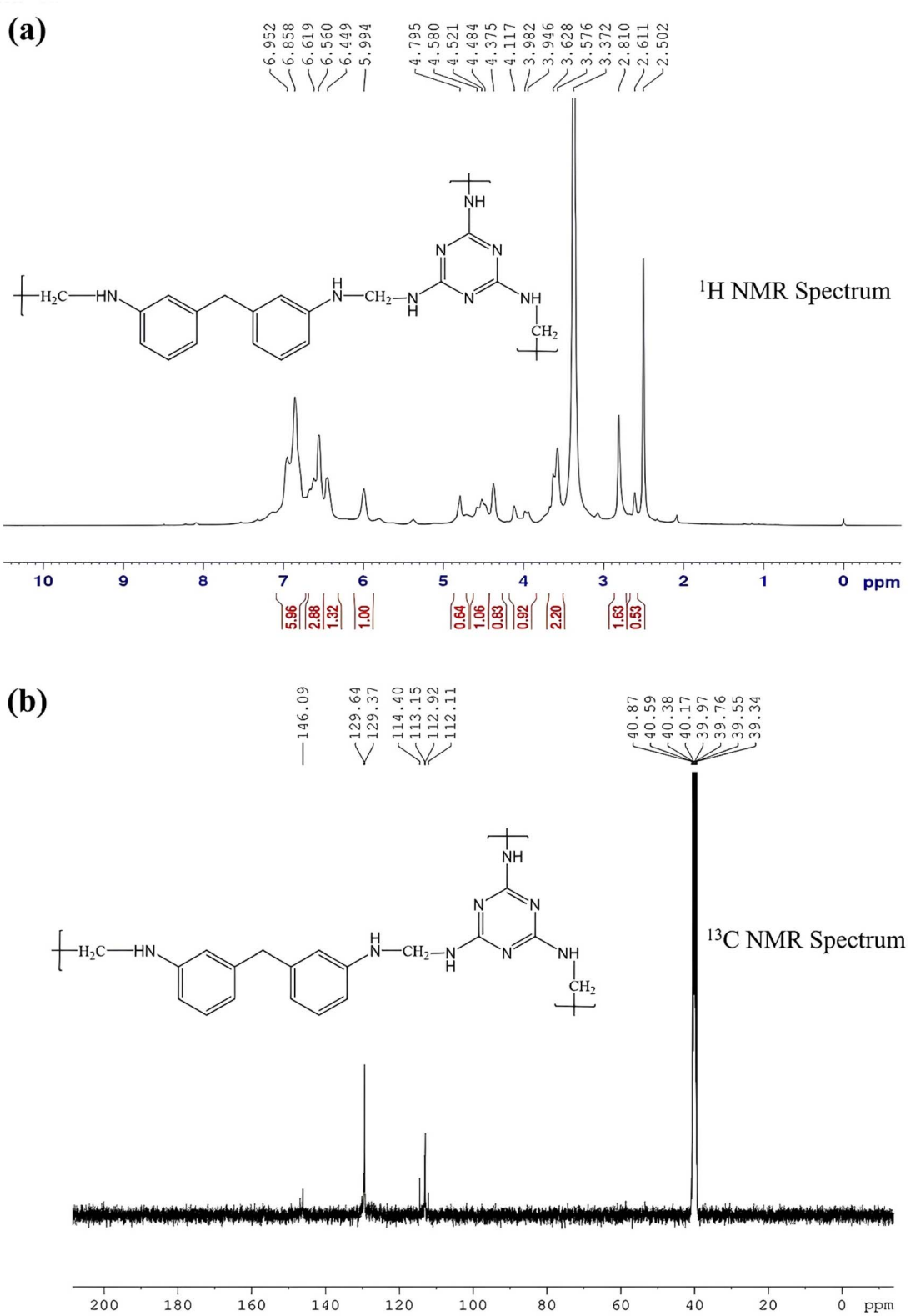

Fig. 3 Experimental (a) ^{1}H and (b) ^{13}C NMR spectra of DMF terpolymer.

3.2.1.3. Electrochemical impedance spectroscopy (EIS). Measurements utilizing EIS provide an efficient way to study interacting patterns over the mild steel interface. Capacitive semicircles are seen over the whole frequency range in the Nyquist plot for metal dipped in 1 M HCl solution under uninhibited and inhibited settings (Fig. 6). Improved inhibition

Table 3 Theoretical NMR spectrum shifts (δ in ppm) for DMF terpolymer

^{1}H atom	δ theoretical	^{13}C atom	δ theoretical
28H	3.63	1C	163.05
29H	3.47	2C	117.87
30H	3.37	3C	141.49
31H	3.44	4C	129.76
32H	7.14	5C	157.89
33H	8.08	6C	126.68
34H	6.94	7C	54.93
35H	7.57	8C	158.72
36H	4.47	9C	131.65
37H	4.59	10C	142.29
38H	7.39	11C	117.73
39H	7.39	12C	160.65
40H	8.06	13C	129.44
41H	7.40	14N	4.03
42H	5.59	15C	39.07
43H	5.88	16N	30.74
44H	5.32	17C	59.43
45H	6.10	18N	46.40
46H	4.66	19C	178.84
47H	4.65	20N	130.98
48H	4.58	21C	178.22
49H	3.27	22N	132.87
50H	3.27	23C	177.46
51H	4.32	24N	125.66
52H	3.48	25N	18.34
—	—	26N	24.52
—	—	27C	36.17

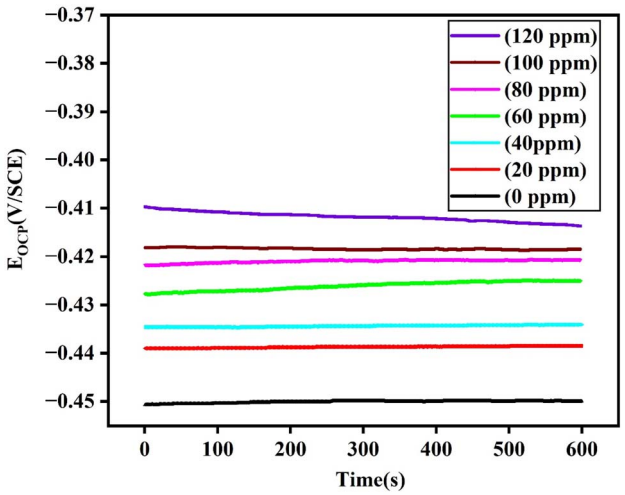

Fig. 4 OCP curves of mild steel immersed in 1 M acid, recorded with different concentrations of DMF.

effectiveness is shown by the semicircle's radius, which is noticeably bigger when inhibiting agents are present than in the blank solution and rises at higher inhibitor doses. The correlation among the corrosion process's charge transfer resistance and double-layer capacitance capability are illustrated using a single capacitive loop. Since Nyquist plots only demonstrate one semicircle, it is certainly possible that a single charge

Table 4 LPR variables for mild steel submerged in 1 M HCl using varying amounts of DMF polymer

Conc. (ppm)	E_{corr} (mV (SCE))	I_{corr} (μA cm^{-2})	R_p (Ω cm^2)	IE (%)
Blank	−449.2	754	30.14	—
20	−426.9	428	53.4	43.56
40	−404.7	300.1	84.6	64.37
60	−425.1	211	115.4	73.88
80	−422.1	115	256.2	88.24
100	−417.5	52	386	92.19
120	−429.11	46	436.2	93.09

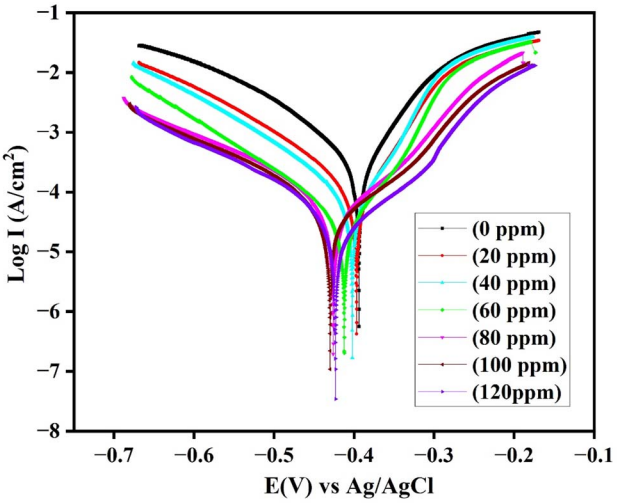

Fig. 5 Tafel plot for mild steel immersed in acidic medium at different DMF amounts.

transfer procedure is accountable for mild steel's HCl deterioration. The mild steel surface's unevenness and frequency dispersion are blamed for the imperfection of semicircles.

The findings from the Nyquist plot were further substantiated by the Bode curves. It was found that the inhibitor-containing solutions loop sizes were bigger than those of the blank solution, and that these sizes grew as the quantity of inhibitor increased. This is attributed to the surface coverage by adsorptive protecting groups from the inhibitors on the mild steel substrate.

Impedance behavior is typically interpreted utilizing a Randle circuit, as illustrated in Fig. 6. This system comprises solution resistance (R_s), a constant phase element (CPE), and charge transfer resistance (R_{ct}). The CPE value, whose exponential factor n indicates distinct electrical characteristics, provides significant understanding into the creation of the double layer at the substrate contact.[31] In particular, resistance, Warburg impedance, capacitance, and inductance are represented by the values of n', which are 0, 0.5, 1, and −1, accordingly. The following formula was utilized to determine the CPE's impedance:

$$Z_{CPE} = Y_o^{-1}(i\omega)^{-n}$$

Table 5 PDP variables for mild steel submerged in 1 M HCl using varying amounts of DMF terpolymer

Conc. (ppm)	β_a (mV dec^{-1})	β_c (mV dec^{-1})	E_{corr} (mV (SCE))	I_{corr} (μA cm^{-2})	IE (%)
Blank	64	106.1	−396	451	—
20	62.1	107.5	−404	228.1	49.42
40	64	106.4	−403	154.4	65.76
60	70.6	111.1	−415	119.2	73.57
80	109	126	−416	69.8	84.52
100	121	136	−422	30.5	93.24
120	115	125	−420	26.6	94.10

where the variable ω stands for angular frequency, Y_o refers to the CPE constant, and n is the deviation indicator associated with mild steel substrate uniformity. According to the current study, the CPE mostly functions as a capacitor, with readings that are close to 1 in both inhibitor free solution and the solution containing inhibitor. Additionally, charge transfer resistance (R_{ct}), inhibiting effectiveness, and double layer capacitance (C_{dl}) were evaluated by applying these EIS results. The double-layer capacitance (C_{dl}) may be computed using the following formula from the CPE.

$$C_{dl} = (Y_o R_{ct}^{1-n})^{1/n}$$

The findings unequivocally show that introducing inhibitor to 1 M hydrochloride enhances the R_{ct} values while diminishing the C_{dl} readings compared to the inhibitor-free solution. The inhibitor's binding onto the steel interface subsequently triggers the decrease in C_{dl}. Furthermore, the drop in C_{dl} correlates with a spike in the electrical double layer's thickness and a decline in the local dielectric constant owing to the inhibitory compound's adsorption. Table 6 illustrates that the presence of inhibitor results in greater R_{ct} values compared to the blank solution. Because of the inhibiting molecule adsorption, there are less unoccupied active locations on the steel substrate, as seen by an elevation in R_{ct} values as the inhibitor concentration increases. This suggests that a protective coating has formed on the working steel electrode surface. This barrier lessens the possibility of metal interaction with chloride ions. Notably, the existence of the inhibitor causes the n value to rise, indicating a reduction in surface inconsistency as a result of the inhibiting agent's adsorption.

Bode graphs of metal samples submerged in corrosive settings in inhibitor-free solution and with inhibitor solution are shown in Fig. 6. The results reported here are consistently supported by Bode graphs, which show single maxima and illustrate that the phase angle increases with rising amounts of inhibitor and reaches peak values at lesser frequency levels. This rise in the phase angle raise suggests that the steel's surface has developed a stronger insulating coating, which adequately resists deterioration.

3.2.2. Adsorption isotherm. The majority of inhibitors reduce deterioration primarily through the adsorption method. The binding of inhibitory agents in an acidic setting act through quasi-substitution procedure, wherein these molecules replace chloride ions and water molecules, as metal surfaces are usually coated with a film of bonded chloride ions and water molecules. In this context, a more accurate adsorption model is found through fitting experiment findings with various isotherms, including the Langmuir-, Frumkin-, and Temkin isotherms.[32] The Langmuir adsorption isotherm fits the data most effectively among all isotherms, providing a linear regression coefficient that is almost equal to unity (Fig. 7). Below is an equation that depicts this isotherm:

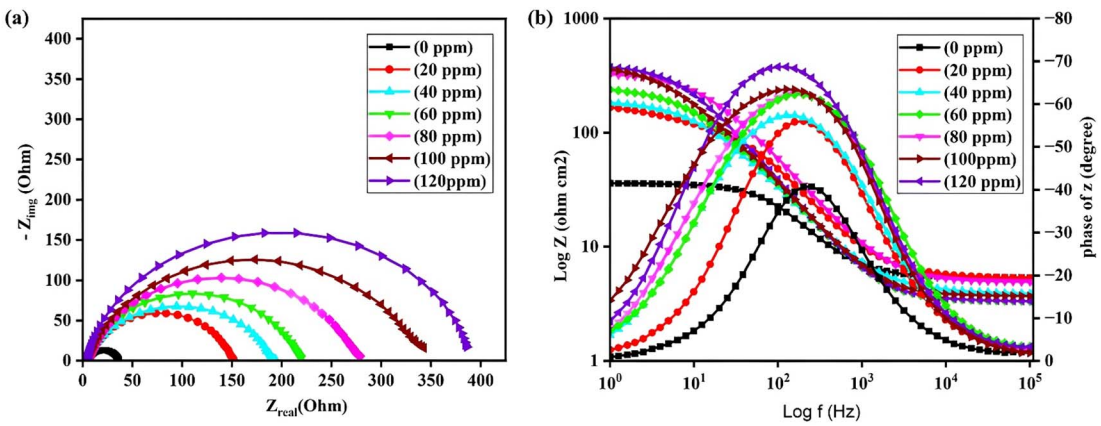

Fig. 6 (a) Nyquist and (b) Bode plots for mild steel dipped in 1 M HCl at different DMF terpolymer amounts.

Table 6 EIS variables for mild steel dipped in 1 M HCl using varying amounts of DMF terpolymer

Conc. (ppm)	R_s (Ω cm^2)	R_{ct} (Ω cm^2)	Y_o (10^{-6} Ω^{-1} cm^{-2})	n	C_{dl} (μF cm^{-2})	IE (%)
0	5.04	30.71	287.70	0.853	1377.18	—
20	5.07	144.75	192.30	0.88	776.35	43.63
40	5.14	190.23	145.84	0.896	478.19	65.28
60	5.20	214.20	126.90	0.902	384.80	72.06
80	5.39	273.34	76.78	0.911	202.99	85.26
100	5.85	337.66	42.20	0.935	82.05	94.04
120	6.31	382.663	36.10	0.937	68.53	95.02

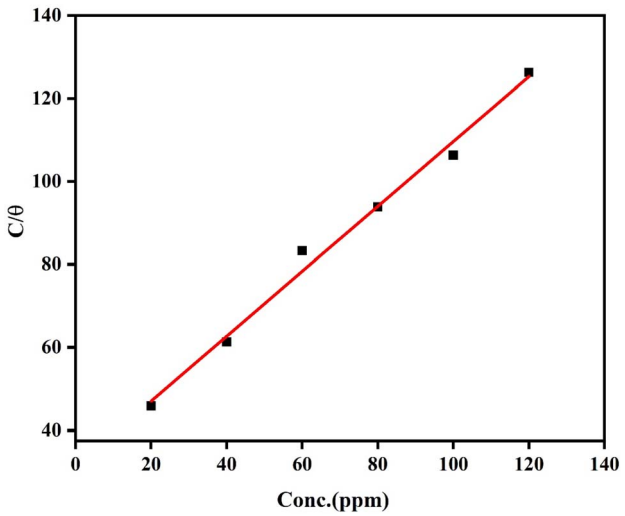

Fig. 7 Langmuir adsorption isotherm curve for DMF terpolymer on mild steel.

$$\frac{C}{\theta} = \frac{1}{K_{ads}} + C$$

where K_{ads} is the equilibrium constant of the adsorption procedure, θ is surface coverage, and C is the inhibitor amount.

Additionally, the inverse of the intercept from the C/θ *vs.* C graph is utilized to ascertain the value of K_{ads}. The ΔG_{ads} for inhibitor adhesion is then calculated employing this value in additional computations.

$$\Delta G_{ads} = -2.303RT\log(10^6 K_{ads})$$

The less than zero value of Gibbs free energy signifies spontaneous binding, which also enhances the stability of the formed layer over the metallic substrate. A greater capacity of the inhibitor to adhere onto metallic surfaces in the acidic atmosphere is shown by a larger ΔG_{ads} value. Gibbs free energy readings beyond -40 kJ mol^{-1} display chemical adsorption with a chemical connection among metallic substrate and inhibitory atoms, whereas readings approximately beneath -20 kJ mol^{-1} point to physical adsorption owing to electrostatic interactions.[33] The inhibitor displays both physical and chemical adsorption. This pattern is confirmed by the negative ΔG_{ads} values (>-40 kJ mol^{-1} and <-20 kJ mol^{-1}) in Table 7.

Table 7 Calculated Gibbs free energy of adsorption (ΔG_{ads}) value for the adhesion of DMF over mild steel

Slope	R^2	K_{ads}	ΔG_{ads} (kJ mol^{-1})
0.78	0.99085	0.0319	26.56

3.2.3. Surface study: AFM. Using AFM analysis, the effect of introducing inhibitors to an HCl solution on the mild steel surface morphology is evaluated. By establishing a barrier of protection across the surface, inhibitors work to mitigate metal corrosion.[34] Thus, further verification of the efficacy of the selected inhibitor may be obtained by comparing the surface features of steel surfaces that are protected and those that are not. Polished mild steel has shown a roughness of 2.735 nm. AFM pictures of the metallic surface taken 3 h after being submerged in the inhibited and blank settings are displayed in Fig. 8. A badly damaged and extensively deteriorated metal surface caused by acidic species getting accessibility to the exposed steel can be seen with a roughness of 267 nm (Fig. 8d). The destructive nature of the hydrochloride (HCl) solution can be greatly decreased by adding a higher amount of DMF inhibitor, which will shield the metal against degradation. This is seen by the shielded metal's smooth and orderly shape in Fig. 8f with a roughness of 65 nm. This decline in roughness of metallic substrate upon introducing inhibitor shows mitigation in the pace of corrosion. This is mostly because when the steel electrode surface comes into touch with the inhibitory agent, a coating of protection forms on it, which prevents its contact with corrosive species.

3.2.4. Theoretical study: DFT. Density Functional Theory (DFT) sought to improve our understanding of the interactions among inhibitor molecules and metallic substrate at a molecular level. DFT was utilized in gaseous state to investigate molecular structures, correlate the data with the experimental results, and assess the impact of electronic density on inhibitor adsorption over metal. Considering many factors such as the energy of the frontier molecular orbitals (FMOs) E_{HOMO} and E_{LUMO}, energy separation among FMO (ΔE), global hardness and softness, the inhibiting substances optimal compositions and locations of activity for adhesion were found in accordance with DFT.[35]

The study looked at the inhibitor's capacity to take in protons in an acidic setting. It was discovered that the characteristics and actions of compounds were altered when hydrogen

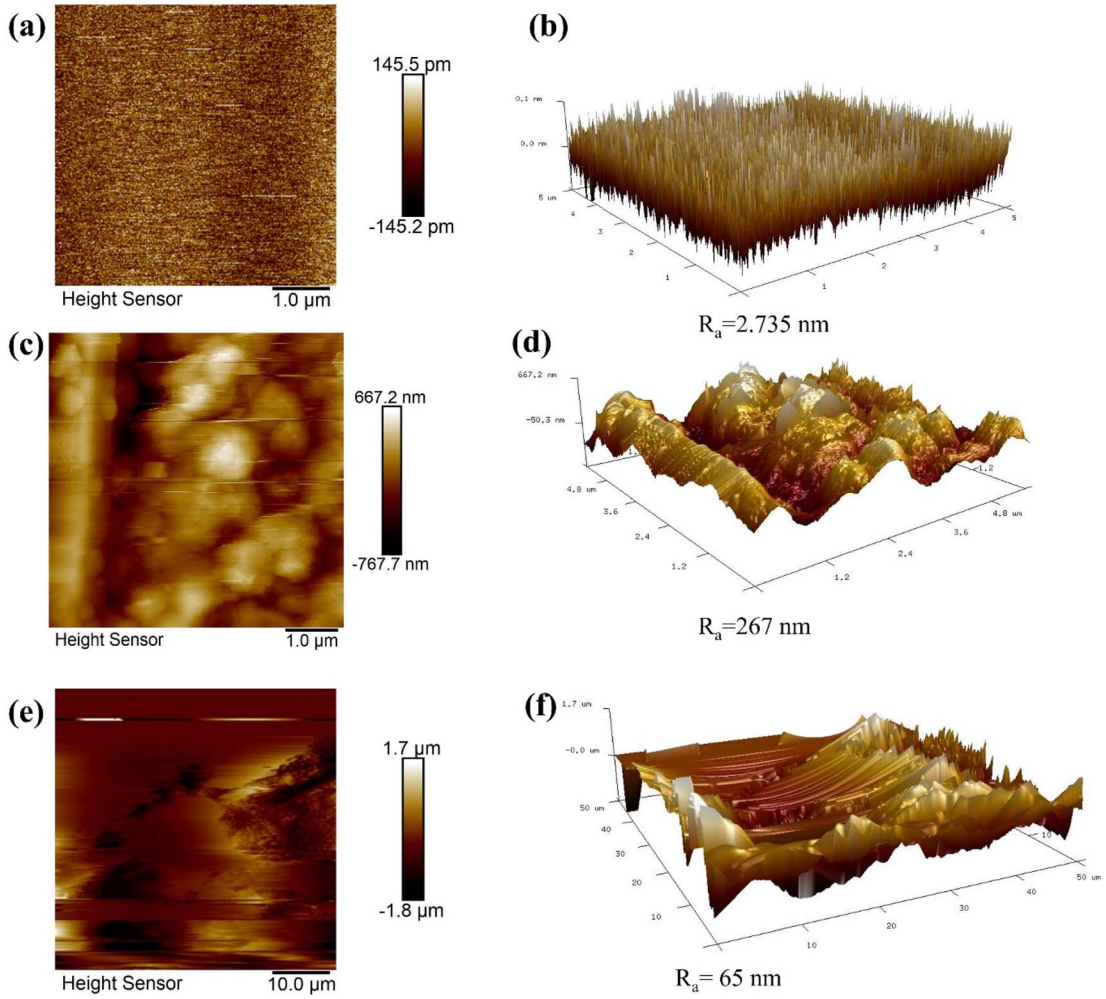

Fig. 8 (a) and (b) 2D and 3D images, respectively, of polished mild steel; (c) and (d) 2D and 3D images, respectively, of mild steel submerged in 1 M HCl; (e) and (f) 2D and 3D AFM images, respectively, of mild steel after treatment with DMF terpolymer.

Table 8 DFT parameters for DMF and protonated DMF terpolymer

Parameters	DMF	Protonated DMF
HOMO	−8.194	−8.104
LUMO	−4.601	−4.688
ΔE	3.593	3.416
μ	−6.397	−6.396
I	8.194	8.104
A	4.601	4.688
η	1.796	1.708
σ	0.557	0.585
χ	6.397	6.396
ω	36.759	34.939
ΔN	−1.417	−1.346
Dipole moment	3.096	8.009

atoms were added to the compound's nitrogen heteroatom, specifically 52H over 16N of DMF polymer. According to Table 8, the protonated state of the inhibitor was more efficient. The active sites were changed by the addition of hydrogen atom (52H) over nitrogen (16 N) which affected the pattern of electron density displayed by the HOMO, LUMO, and ESP maps in Fig. 9.

The characteristics linked to the LUMO and HOMO orbitals are the only ones needed for exploring the binding process. The HOMO and LUMO correspond to distinct places with differing propensities to donate or receive electrons with the metallic surface. The willingness to provide electrons is effectively represented by the HOMO energy (E_{HOMO}); the larger the number, the stronger the ability to donate electrons. Conversely, the smaller the LUMO energy (E_{LUMO}), the more efficient is the ability to acquire electrons. Additionally, a lower ΔE promotes inhibitor-metallic binding.[36]

It is evident that the chemical reactivity of the neutral species (DMF) is influenced by the protonation of the nitrogen atom. As per documented patterns of inhibitory efficacy, the research findings indicate that the protonated polymer appears more reactive than the neutral polymer molecule, as confirmed by a reduction in ΔE values following protonation, with the ΔE value observed in the order of DMF > protonated DMF.

The inverse relationship of hardness (η) and softness (σ) is an essential variable in chemical adherence to metallic

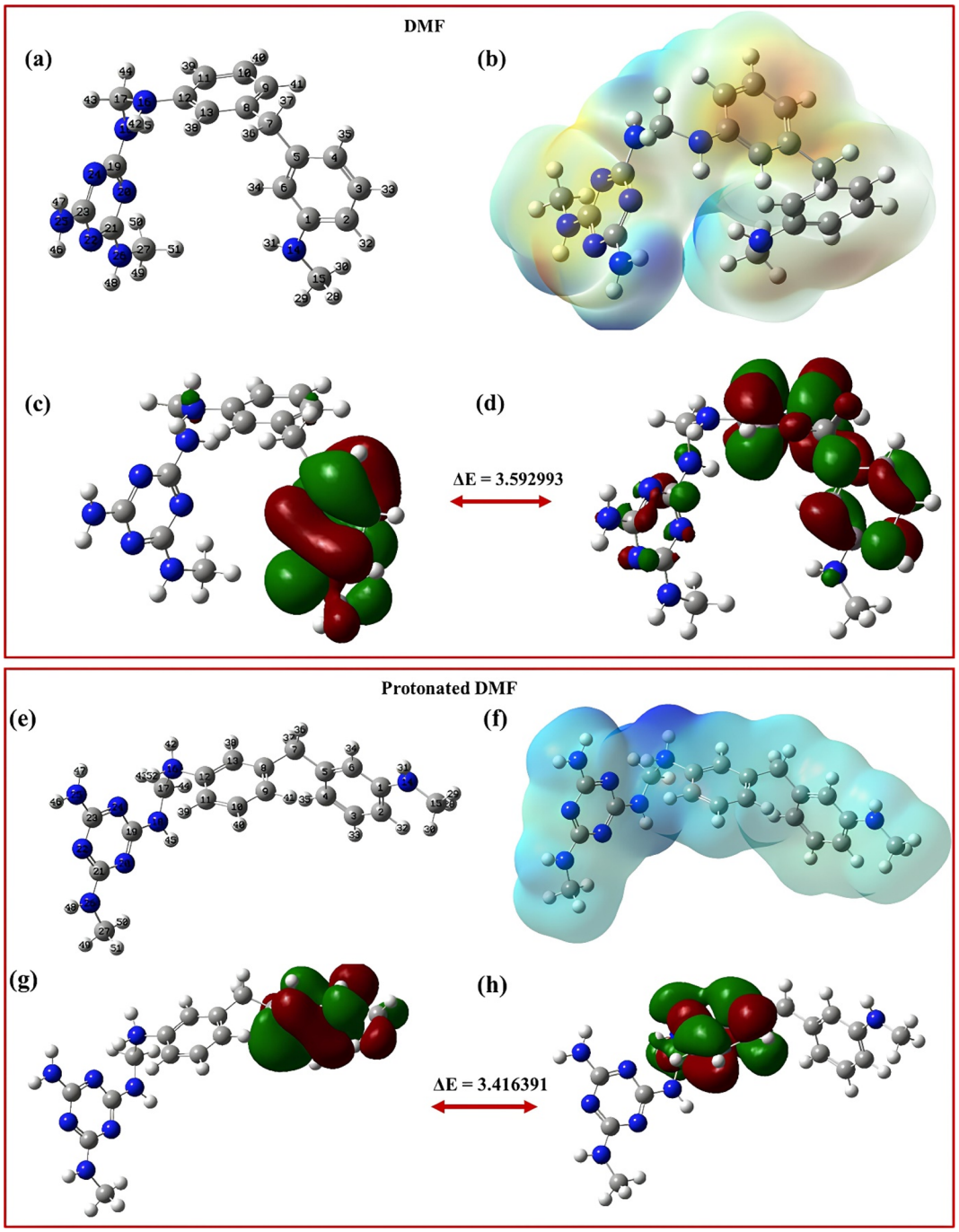

Fig. 9 Optimised structure (a and e); ESP distribution (b and f); HOMO (c and g) and LUMO (d and h) for DMF and protonated DMF terpolymer respectively.

substrates. Softer inhibitors are more potent, especially when used with iron, which is regarded as a soft acid, in accordance with the hard and soft acids and bases (HSAB) hypothesis. This idea is upheld by DMF and protonated DMF, which are distinguished by decreased hardness and increased softness on protonation. These outcomes demonstrate that the protonated form is more reactive than the neutral form of polymer and the polymer forms coordinated bonds with mild steel and forms a protective layer.

A molecule's inclination for attracting electrons is measured by the electrophilicity index (ω). An elevated ω indicates a greater propensity towards receiving electrons. From Table 8 statistics, it can be deduced that protonated DMF has a larger ω; therefore, it has higher interacting and inhibiting properties.

The dipole moment (μ) plays a key role in understanding how organic inhibitors work to prevent corrosion. According to Table 8, the high dipole moment of protonated DMF may enhance its adsorption onto the iron surface. Also, the higher

dipole moment of the DMF molecule can strengthen its adsorption on steel and facilitate electron transfer from the protonated molecule to the metal.

These outcomes confirm the previously noted trends in the DFT parameters. The protonated state of the polymer was more efficient than the neutral state.

The molecular electrostatic potential (ESP) was calculated to assess local reactivity (active locations). The ESP often depicts sections with different electron densities like low-density positive zones (blue), high-density negative zones (red), and medium-density intermediate zones (many different hues).[37] It is clearly seen that the highest negative potential, which is coloured in red, surrounds the heteroatom nitrogen and aromatic rings and is a good indicator of the amount of electrons present as well as possible locations where coordinate adhesion connections may occur. Additionally, a blue-shaded region is prominent at different locations in the studied compound, highlighting a lack of electrons and probable locations for physical adhesion involving electrostatic bonds. The chemical structure has a positive charge upon protonation, indicating the molecule's capacity for electrostatic interactions and for taking up electrons. The combination of these outcomes demonstrates that both DMF and protonated DMF compounds have reactive electron donor and acceptor regions, which are important in achieving powerful adhesion over the metallic surface.

The inhibiting molecule's binding point is identified by Mulliken atomic charges. A negative value suggests that there is a high probability of providing electrons towards the metallic surface's unoccupied orbital. An essential feature of a successful corrosion inhibitor is the inhibiting molecule's capacity to supply electrons to the metallic substrate, which is highlighted through its negative charge. A notable amount of negative charge has been observed in the atoms 24 N, 20 N, 22 N, 14 N, and 26 N for the DMF molecule and protonated DMF molecules (Table 9). The compounds preferred site for binding is represented through these atoms. It seems that the nitrogen atoms and aromatic rings gives the compounds under investigation their higher inhibitory efficiency.

Additionally, the individualized nature and reactivity of inhibitor atoms can be assessed by employing Fukui functions which indicate the active atoms or locations for adsorption. Such possible places maintain inhibiting species close to the specimen's surface by facilitating connections among donors and acceptors.[38] The electrophilic and nucleophilic inclinations of structural locations are represented by the indices f_k^- and f_k^+, respectively. Greater responsiveness is indicated by larger values for such indices. There areas are known as electrophilic sites and nucleophilic sites wherein electrons have a greater probability to be received or provided, respectively. The variables obtained through this investigation are compiled in Fig. 10. The findings indicate that the f_k^+ values for C (17), N (16), C (9), C (13), N (18), and N (14) atoms for neutral DMF and N (14), C (4), C (15), C (2), 6 (C) in protonated DMF are significantly greater compared to other DMF framework atoms. This suggests that these atoms are candidates for nucleophilic attacks. The atoms C (6), C (3), C (19), C (23), N (25), C (12) in the neutral DMF and C (17), C (9), N (16), N (25), C (19) in protonated DMF are the most favoured sites for an electrophilic attack because they have the largest value of f_k^-. The protonated form shows several electron-acceptor sites, while the electron-donor sites have notably diminished. Furthermore, most of the locations are distributed across the entire framework of the protonated molecule. The inhibiting agent DMF forms a thick deterioration-preventive barrier over the metallic surface by utilizing such electron exchanging capability based on the analysis of reactive sites.

Table 9 Mulliken charges on DMF and protonated terpolymer atoms

Atoms	DMF	Protonated DMF
1C	0.165745	0.092855
2C	−0.00849	0.029051
3C	−0.01538	0.022688
4C	−0.01825	−0.03226
5C	−0.10932	−0.11724
6C	0.032686	0.042816
7C	0.103892	0.163745
8C	−0.12399	−0.12525
9C	0.021434	0.172283
10C	−0.01309	0.032059
11C	−0.02006	0.024849
12C	0.173079	0.065488
13C	−0.01323	0.072464
14N	−0.23696	−0.19068
15C	0.150302	0.15811
16N	−0.22021	0.239016
17C	0.285694	0.203127
18N	−0.19781	−0.10473
19C	0.477307	0.46134
20N	−0.42965	−0.37882
21C	0.461826	0.427636
22N	−0.42406	−0.36064
23C	0.433582	0.43359
24N	−0.45485	−0.43409
25N	−0.01097	0.042328
26N	−0.20288	−0.13156
27C	0.193657	0.191808

3.3. Antimicrobial study

Using the disc diffusion method and streptomycin as a reference antibiotic, the antimicrobial activity of the DMF terpolymer was assessed. *Staphylococcus aureus*, *P. aeruginosa*, and *B. subtilis* were tested for resistance to the prepared compounds.

The test results, which are shown in Table 10, indicated that these bacteria were actively inhibited from growing by the DMF terpolymer, proving that the DMF terpolymer possess good antibacterial activity.

The human and ruminant gastrointestinal tracts harbor the Gram-positive, rod-shaped bacterium, *S. aureus*. DMF terpolymer demonstrated excellent activity against *S. aureus* and *B. subtilis* (Fig. 11). This is owing to DMF's lipophilic nature, favoring permeation through the bacterial membranes' lipid layers. It is thought that solubility, conductivity, dipole moment, and cell permeability may also be responsible for the

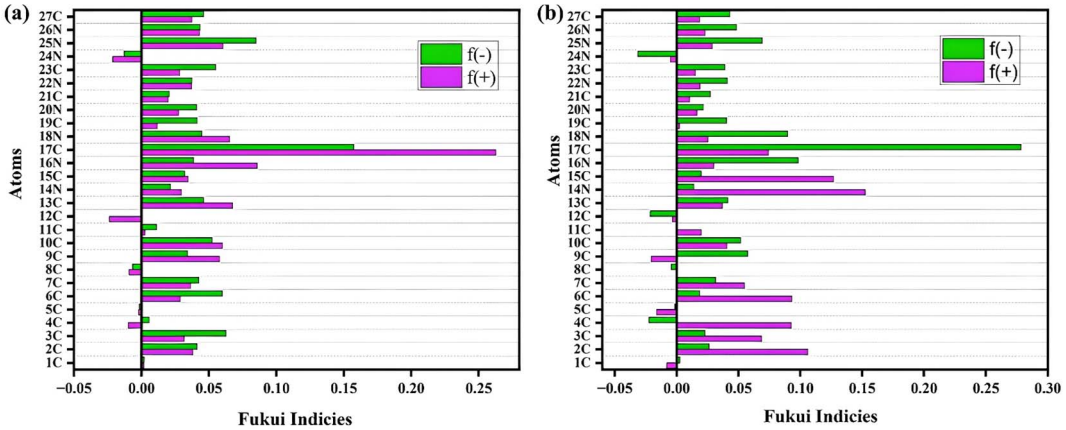

Fig. 10 Fukui indices for DMF (a) and protonated DMF (b) terpolymer atoms.

Table 10 Antimicrobial results of DMF terpolymer ligand

Sample	Organisms	10 mg mL^{-1}	20 mg mL^{-1}	30 mg mL^{-1}	40 mg mL^{-1}	Streptomycin
DMF	*S. aureus*	13	14	15	16	21
	P. aeruginosa	13	13.5	15	17	22
	B. subtilis	12	13	15	16.5	22

DMF's increased activity. The antibacterial properties of the terpolymer were also attributable to the nitrogen donor group that was present in the polymer backbone.

3.4. Comparison of corrosion inhibition efficiency

Table 11 presents a comparative analysis of DMF terpolymer with other polymer-based corrosion inhibitors from the literature. Notably, the DMF terpolymer demonstrates excellent inhibition efficiency at relatively low concentrations, making it a promising candidate for corrosion protection. The 4,4-diaminodiphenylmethane-melamine-formaldehyde (DMF) terpolymer achieves 94% inhibition efficiency at just 100 ppm in 1 M HCl, outperforming several reported inhibitors in acidic environments.

4. Mechanism of inhibition

The DMF terpolymer corrosion inhibition mechanism on mild steel in hydrochloric acid (HCl) environment is essentially determined by its molecular makeup and concentration. This polymer effectively reduces deterioration by tightly sticking to the steel substrate *via* two distinct processes: chemical adsorption (coordinate bonding) and physical adsorption (electrostatically) (Fig. 12).

Chemically, the polymer molecules include heteroatoms (nitrogen) with lone pairs of electrons and π-electrons from aromatic rings are capable of interacting with the unoccupied d-orbitals of iron atoms on the steel substrate. Furthermore, the back-donation mechanism involves the transfer of electron

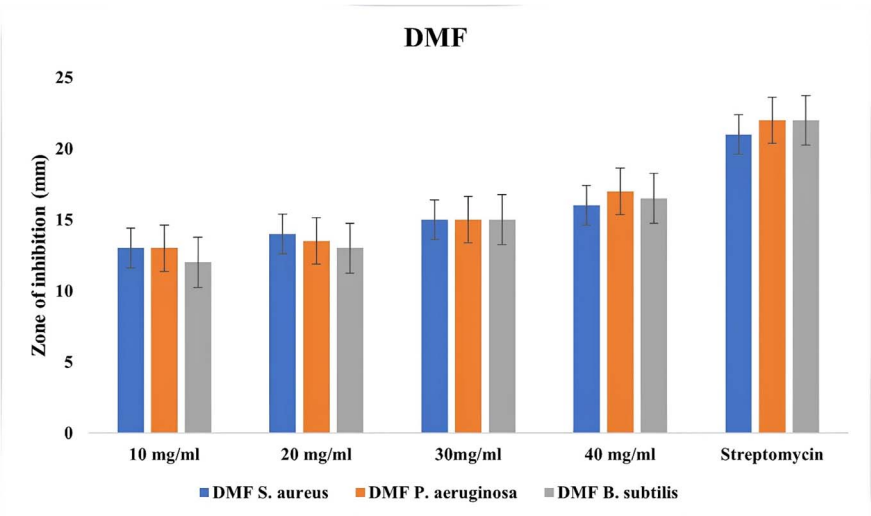

Fig. 11 Antimicrobial screening of DMF terpolymer ligand.

Table 11 Comparison of corrosion inhibitor performance with other polymers

Compound	Inhibition efficiency	Concentration and medium	Ref
(*p*-Semidine-guanidine-formaldehyde) terpolymer	93.7% mild steel	10^{-3} M in H_2SO_4	19
Acrylic acid (AA), oxalic acid-allypolyethoxy carboxylate (APEM)-phosphorous acid (H_3PO_3) terpolymer	79.77% carbon steel	30 mg L^{-1} in 1 M HCl	39
Chitosan-acrylic acid-polysuccinimide terpolymer	71.17% carbon steel	500 mg L^{-1} in 3.5% NaCl	40
Acrylamide/styrene/maleic anhydride terpolymers (ASM) and thermally aged acrylamide/styrene/maleic anhydride terpolymers (A/ASM)	ASM (52%), A/ASM (94%)Mild steel	3000 ppm in 3.5% NaCl	41
4,4-Diaminodiphenylmethane-melamine-formaldehyde terpolymer (DMF)	94% mild steel	100 ppm in 1 M HCl	Present work

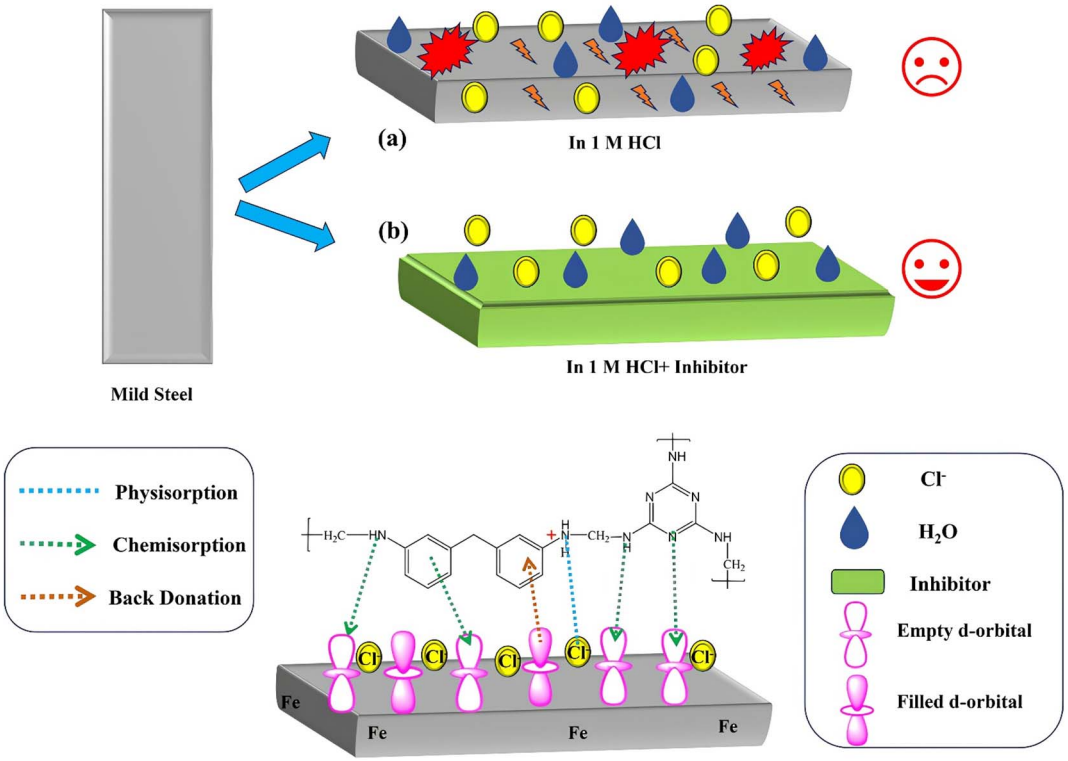

Fig. 12 Mechanism of corrosion inhibition by DMF terpolymer.

density from the filled d-orbitals of Fe atoms to the vacant antibonding orbitals of the polymer π-conjugated system. This contact causes the polymer molecules to establish persistent coordination bonds, enabling them to stick tightly to the steel and create a protective layer. In an acidic hydrochloric acid surrounding, chloride ions (Cl^-) deposited on the steel substrate create a negative charge on the metallic material. At the same time, the heteroatom N in polymer molecules are protonated, gaining a positive charge. This causes electrostatic interactions among the positively charged polymer molecules and the negatively charged steel substrate to enhance the adhesion mechanism. Together, these chemical and physical processes generate a long-lasting protective coating over the steel, prohibiting corrosive substances from accessing the surface and considerably reducing corrosion.

5. Conclusion

This study focused on the synthesis and characterization of 4,4-diaminodiphenylmethane-melamine-formaldehyde terpolymer (DMF), investigating its corrosion inhibition properties for mild steel in 1 M HCl solution. The terpolymer was synthesized *via* condensation polymerization and characterized using FTIR, ^{1}H NMR, and ^{13}C NMR spectroscopy, with its molecular weight determined by gel permeation chromatography. The study establishes the DMF terpolymer as a highly effective corrosion inhibitor for mild steel in hydrochloric acid, providing comprehensive insights from both experimental and computational perspectives.

(1) Electrochemical tests including PDP and EIS demonstrated that the DMF terpolymer significantly reduced the

deterioration rate of mild steel in 1 M HCl solution, with excellent inhibitory efficiency of 94% at 100 ppm.

(2) Potentiodynamic polarization examination revealed that the DMF terpolymer effectively functioned as a mixed-kind of inhibitory agent, influencing both anodic and cathodic reactions.

(3) The adsorption of the DMF terpolymer adhered to the Langmuir isotherm model, suggesting that a monolayer of DMF molecules forms on the mild steel surface.

(4) ΔG_{ads} values show that the DMF terpolymer displayed strong adsorption capability through both physical and chemical interaction and robust binding with the steel surface in an acidic environment.

(5) Atomic force microscopy (AFM) surface analysis confirmed the adhesion of the DMF terpolymer onto the mild steel substrate, forming a protective layer that reduced surface roughness from 267 nm to 65 nm and inhibited corrosion.

(6) Density functional theory (DFT) studies revealed that the terpolymer's molecular structure promotes significant adhesion onto the metal surface, which is consistent with the experimental findings and strengthens the terpolymer's efficiency as a corrosion inhibitor.

(7) The terpolymeric ligand had strong antimicrobial action, suppressing the development of *S. aureus*, *P. aeruginosa*, and *B. subtilis*, as proven through the disc diffusion technique.

Data availability

All the data have been included in the manuscript.

Conflicts of interest

The authors state that the integrity of the research described in this paper has not been compromised by any notable financial conflicts or personal ties.

Acknowledgements

RS thanks the CSIR, New Delhi for the research fellowship [File number-09/1256(16056)2022-EMR-I].

References

1 R. Sehrawat and B. Mangla, *Coord. Chem. Rev.*, 2025, **525**, 216346.
2 Y. Y. Li, Z. N. Jiang, X. Wang, X. Q. Zeng, C. F. Dong, H. F. Liu and G. A. Zhang, *Corros. Sci.*, 2022, **209**, 110695.
3 M. Khattabi, F. Benhiba, S. Tabti, A. Djedouani, H. Zarrok, A. Boutakiout, R. Touzani, I. Warad, M. E. Touhami, H. Oudda and A. Zarrouk, *Anal. Bioanal. Electrochem.*, 2023, **15**, 739–766.
4 A. Miralrio and A. E. Vázquez, *Processes*, 2020, **8**, 942.
5 Y. L. Kobzar and K. Fatyeyeva, *Chem. Eng. J.*, 2021, **425**, 131480.
6 D. K. Verma, R. Sahu, E. Berdimurodov, C. Verma, M. A. Quraishi, V. K. Jain and K. Berdimuradov, *J. Mol. Struct.*, 2023, **1294**, 136313.
7 R. Narang, P. Vashishth, H. Bairagi, R. Sehrawat, S. Shukla and B. Mangla, *Adv. Mater. Lett.*, 2023, **14**, 2304–1732.
8 P. Vashishth, H. Bairagi, R. Sehrawat, S. K. Shukla and B. Mangla, *J. Mol. Liq.*, 2024, **403**, 124799.
9 D. A. Winkler, A. E. Hughes, C. Özkan, A. Mol, T. Würger, C. Feiler, D. Zhang and S. V. Lamaka, *Prog. Mater. Sci.*, 2025, **149**, 101392.
10 R. Sehrawat, P. Vashishth, H. Bairagi, S. K. Shukla, H. Kumar, G. Ji and B. Mangla, *Coord. Chem. Rev.*, 2024, **514**, 215820.
11 M. Akrom, S. Rustad, A. G. Saputro and H. K. Dipojono, *Comput. Theor. Chem.*, 2023, **1229**, 114307.
12 A. A. Al-Amiery, W. N. R. W. Isahak and W. K. Al-Azzawi, *Lubricants*, 2023, **11**, 174.
13 A. G. Sayed, A. M. Ashmawy, W. E. Elgammal, S. M. Hassan and M. A. Deyab, *Sci. Rep.*, 2023, **13**(1), 1–23.
14 M. Eissa, S. H. Etaiw, E. E. El-Waseef, A. El-Hossiany and A. S. Fouda, *Sci. Rep.*, 2024, **14**(1), 1–20.
15 C. Verma and M. A. Quraishi, *Int. J. Corros. Scale Inhib.*, 2021, **10**, 851–860.
16 H. Bairagi, P. Vashishth, R. Sehrawat and B. Mangla, *Can. Metall. Q.*, 2024, 1–40.
17 A. A. Javidparvar, A. Farhadian and A. R. Shahmoradi, *Grafted Biopolymers as Corrosion Inhibitors: Safety, Sustainability, and Efficiency*, 2023, pp. 337–363.
18 S. M. Chhipa, S. Sharma and A. Kumar Bagha, *Mater. Today: Proc.*, 2024, DOI: **10.1016/J.MATPR.2024.09.001**.
19 B. Arifa Farzana, N. Mujafarkani, A. Thakur, A. Kumar, A. Mushira Banu and M. Shifana, *Inorg. Chem. Commun.*, 2023, **158**, 111572.
20 A. Ouass, M. Galai, M. Ouakki, E. Ech-Chihbi, L. Kadiri, R. Hsissou, Y. Essaadaoui, A. Berisha, M. Cherkaoui, A. Lebkiri and E. H. Rifi, *J. Appl. Electrochem.*, 2021, **51**, 1009–1032.
21 M. Abdallah, A. Fawzy, H. Hawsawi, R. S. A. Hameed and S. S. Al-Juaid, *Int. J. Electrochem. Sci.*, 2020, **15**, 8129–8144.
22 A. Bendi, A. Jafar Ahamed, T. Jaison Jose, N. Raghav, N. Mujafarkani and S. Atri, *J. Mol. Liq.*, 2024, **408**, 125403.
23 N. Mujafarkani, F. M. M. Ahamed, M. Afshari and S. A. C. Carabineiro, *Int. J. Polym. Mater. Polym. Biomater.*, 2024, **73**(18), 1593–1604.
24 N. Mujafarkani and A. J. Ahamed, *Mater. Today: Proc.*, 2021, **47**, 1920–1928.
25 R. Narang, P. Vashishth, H. Bairagi, R. Sehrawat, S. K. Shukla and B. Mangla, *Chem. Afr.*, 2024, 1–17.
26 R. K. Mehta, S. K. Gupta and M. Yadav, *J. Environ. Chem. Eng.*, 2023, DOI: **10.1016/j.jece.2022.108499**.
27 A. Ait Mansour, B. El-Haitout, R. J. Adnin, H. Lgaz, R. Salghi, H. S. Lee, M. R. Alhadeethi, M. Messali, K. Haboubi and I. H. Ali, *Metals*, 2023, **13**, 797.
28 N. Mujafarkani, D. C. Agurokpon, R. A. Hussien, O. V. Ayoola, I. F. Alshdoukhi, G. Sampathkumar, A. A. Alodhayb, S. E. Ogbodo, I. Benjamin, A. J. Ahamed, R. O. Ogar and H. Louis, *J. Mol. Struct.*, 2024, **1298**, 137005.
29 M. A. Ojong, N. Mujafarkani, F. A. K. Khazaal, A. S. Hussam, O. C. Godfrey, K. Muzammil, A. J. Ahamed, R. U. Edadi,

I. A. Anyambula, E. Moses and I. Benjamin, *J. Mol. Struct.*, 2024, **1310**, 138113.
30 R. Sehrawat, R. Pundeer, S. Yadav, P. Vashishth, H. Bairagi, S. K. Shukla and B. Mangla, *J. Mol. Struct.*, 2024, **1316**, 139017.
31 H. Bairagi, P. Vashishth, R. Sehrawat, S. K. Shukla and B. Mangla, *Mater. Chem. Phys.*, 2024, 128958.
32 L. Toukal, M. Foudia, D. Haffar, N. Aliouane, M. Al-Noaimi, Y. Bellal, H. Elmsellem and A. Rahman, *J. Indian Chem. Soc.*, 2022, **99**, 100634.
33 Q. Sun, S. Fu, Y. Peng, P. Li, H. Ma, Z. Fang, T. Ma, R. Zhang, Z. Liang and J. Li, *J. Mol. Struct.*, 2024, **1312**, 138480.
34 A. Farhadian, S. Assar Kashani, A. Rahimi, E. E. Oguzie, A. A. Javidparvar, S. C. Nwanonenyi, S. Yousefzadeh and M. R. Nabid, *J. Mol. Liq.*, 2021, **338**, 116607.
35 R. Sehrawat, S. Yadav, R. Pundeer, D. K. Sharma and B. Mangla, *Prog. Org. Coat.*, 2025, **203**, 109156.
36 A. Kokalj, *Corros. Sci.*, 2021, **193**, 109650.
37 R. Sehrawat, P. Vashishth, V. Chaudhri, R. Pundeer, H. Kumar, E. E. Ebenso and B. Mangla, *Prog. Org. Coat.*, 2025, **198**, 108911.
38 M. Esmaeilzadeh Khabazi and A. Najafi Chermahini, *ACS Omega*, 2023, **8**, 9978–9994.
39 Y. Chen, Y. Zhou, Q. Yao, Y. Bu, H. Wang, W. Wu and W. Sun, *J. Appl. Polym. Sci.*, 2015, **132**(6), DOI: **10.1002/APP.41447**.
40 Y. Zheng, Y. Gao, H. Li, M. Yan, J. Zhao and Z. Liu, *Desalination*, 2021, **520**, 115367.
41 A. Ait Mansour, H. Lgaz, A. Elmoutaouakil Ala Allah, Y. Ramli, M. Messali, H. seung Lee, L. Bazzi, R. Salghi and B. Hammouti, *Mater. Chem. Phys.*, 2024, **320**, 129405.